Supporting Information

Electrochemical Transformation of Prussian Blue Analogues into Ultrathin Layered Double Hydroxide Nanosheets for Water Splitting

Baghendra Singh[a], Om Prakash[b], Pralay Maiti[b], Prashanth W. Menezes[c] and Arindam Indra[a*]

[a]*Department of Chemistry, Indian Institute of Technology (BHU), Varanasi-221005, U.P, India. E-mail: arindam.chy@iitbhu.ac.in*

[b]*School of Material Science and Technology, Indian Institute of Technology (BHU), Varanasi-221005, U.P, India*

[c]*Metalorganics and Inorganic Materials, Department of Chemistry, Technische Universität Berlin, Straße des 17 Juni 135, Sekr. C2, 10623 Berlin, Germany*

Chemicals

The chemicals were acquired from Sigma-Aldrich and Alfa Aesar and used without any further purification. Carbon cloth was purchased from Nara Cell-Tech, Seoul, Korea. Deionised water was used throughout the synthesis, washing and electrochemical measurements.

Instruments

The powder X-ray diffraction (PXRD) of the materials have been recorded on Rigaku D/MAX RINT-2000 X-Ray diffractometer using Cu Kα radiation (λ=1.5418 Å). Elemental analysis was carried out in a Thermo/Flash EA 1112 elemental analyzer. Inductively coupled plasma atomic emission spectroscopic (ICP-AES) measurements were performed in Perkin Elmer-Optima 8300.

Fourier transform-infrared (FT-IR) spectra have been recorded on Thermo Scientific Nicolet iS50 spectrometer. Raman spectroscopic studies have been carried out by using Jasco/NRS-3100 spectrophotometer. X-ray photoelectron spectroscopic measurements have been performed in VG/VG ESCA LAB 220i and data analyses have been carried out using Thermo Avantage software.

The particle morphology was recorded by using field emission scanning electron microscope FEI/NOVA Nano SEM 450. Transmission electron microscopic (TEM) studies were performed in JEOL/JEM-2100F instrument. EDX mapping data were collected from the analyzer attached with the TEM instrument.

Electrochemical measurements have been carried out in Autolab potentiostat/galvanostat (Model PGSTAT-72637).

Experimental

Activation of carbon cloth (CC)[S1]

A piece of carbon cloth (size: 1 cm x 2 cm) was first washed with acetone (2 times) under ultrasonication followed by washing with water for 5 times. The clean carbon cloth was dried at 50 °C for 12 h and treated with concentrated nitric acid for 4 h at 100 °C. The activated carbon cloth was thoroughly washed with deionised water and dried in air oven for 12 h at 50 °C for further use.

Synthesis of cobalt hydroxide carbonate template on carbon cloth (CoFeHC)[S2]

A homogeneous mixture was made by mixing 1 mmol of $CoCl_2 \cdot 6H_2O$, 1 mmol $FeCl_2 \cdot 4H_2O$, 4 mmol NH_4F and 10 mmol of urea in 12 mL deionized H_2O. The mixture was transferred in to a 50 mL Teflon autoclave and a piece of activated carbon cloth was vertically placed to dip 1 cm^2 area inside the solution. The autoclave was sealed and heated at 120 ℃ for 5 h. After natural cooling to room temperature, the CoFeHC film coated carbon cloth was washed with H_2O for 2 times and dried in an oven at 50 °C for 12 h.

Similarly, FeHC was synthesized by changing the metal salt to 2 mmol $FeCl_2 \cdot 4H_2O$ whereas CoHC was prepared from 2 mmol of $CoCl_2 \cdot 6H_2O$.

Synthesis of CoFeCo[S3]

A piece of carbon cloth supported CoFeHC was immersed into 5 mL solution of $K_3[Co(CN)_6]$ (0.2 mmol) in a screw capped glass vial and aged for 10 min at room temperature. The glass vial was capped and placed inside a preheated (60 ℃) oven to heat it for 4 hrs at that temperature. A brown color catalyst film was deposited on carbon cloth. The catalyst film was washed with water for 3 times and dried at 50 ℃ in an air oven for 12 h. Fresh catalyst films were prepared and used every time for the electrochemical experiments.

Similarly, CoCo and FeCo have been synthesized by using CoHC and FeHC templated films on carbon cloth.

Fabrication of RuO_2 on carbon cloth

A catalyst mixture was prepared by dispersing 2 mg commercially available (Sigma) RuO_2 in 200 µL solution containing 100 µL water, 50 µL ethanol and 50 µL of 0.5 wt.% Nafion solution and sonicated for 10 min. The whole amount of the catalyst was drop casted on carbon cloth (25 µL solution every time) and drying at 50 °C for 10 min. The final drying after supporting the whole amount of catalyst on carbon cloth was done at 50 °C in an air oven for 6 h.

Fabrication of 20% Pt/C on carbon cloth

10 mg commercially available 20% Pt/C (sigma) was dispersed in 200 µL solution containing 100 µL water, 50 µL ethanol and 50 µL of 0.5 wt.% Nafion solution and sonicated for 10 min. The whole amount of the catalyst was drop casted on carbon cloth (25 µL solution every time) and drying at 50 °C for 10 min. The final drying after supporting the whole amount of catalyst on carbon cloth was done at 50 °C in an air oven for 6 h.

Table S1. Different catalysts synthesized with their catalyst loading.

Sr. No.	Catalysts	Template on carbon cloth	Cyanometalate reagent	Catalyst loading (mg)
1.	CoFeCo	CoFeHC@CC	$K_3[Co(CN)_6]$	2.9 ± 0.2
2.	CoCo	CoHC@CC	$K_3[Co(CN)_6]$	2.6 ± 0.3
3.	FeCo	FeHC@CC	$K_3[Co(CN)_6]$	2.3 ± 0.2
4.	CoFeHC	CoFeHC@CC	-	2.7 ± 0.1

Electrochemical measurements

Oxygen evolution and hydrogen evolution experiments were performed in a single-compartment three-electrode electrochemical cell in 1.0 M aqueous KOH solution. Catalyst deposited carbon cloth was used as the working electrode and Pt wire was used as the counter electrode. Hg/Hg_2SO_4 electrode was used as the reference electrode in 1 M aqueous KOH solution (pH 14) and the applied potential was represented against reversible hydrogen electrode (RHE) by using the formula:

$$E(RHE) = E(Hg/Hg_2SO_4) + 0.64 + 0.059pH$$

Chronoamperometric measurements were carried out in 1.0 M KOH at constant potential as mentioned in the figures. Correction for i*R* losses and background current was performed for all the CV and LSV measurements whereas chronoamperometric data were represented without any *iR* correction.

Figures

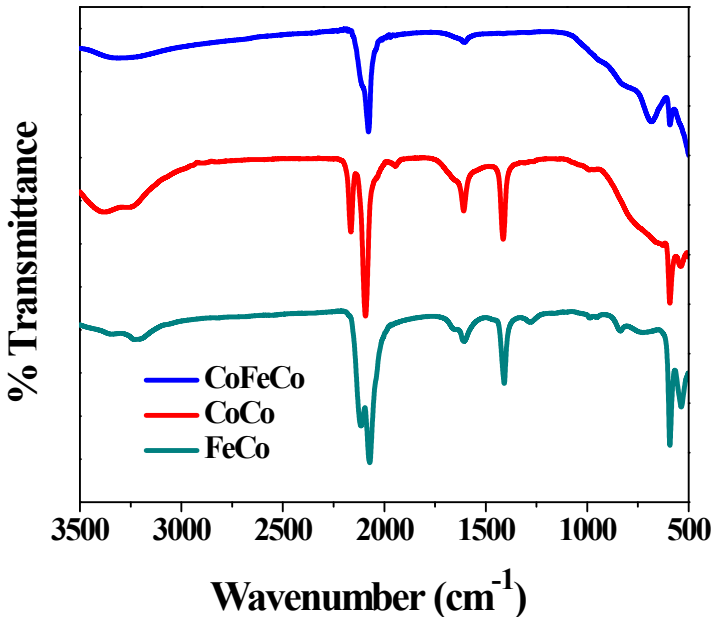

Figure S1. Attenuated total reflection Fourier transformed infrared (ATR-FTIR) spectra of CoFeCo, CoCo and FeCo. The peaks for the stretching vibrations of bridging –CN groups appear in the region 2070-2200 cm^{-1}.[S4] The other peaks arise from the metal hydroxide carbonate template, carbon cloth and water molecules.

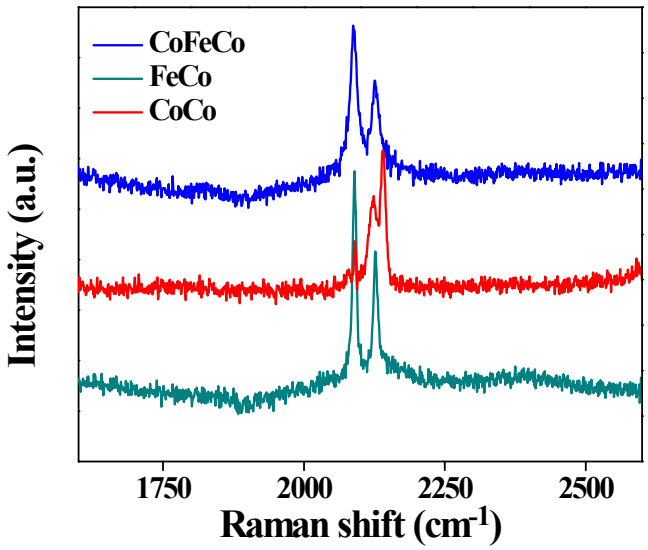

Figure S2. Raman spectra of CoFeCo, CoCo and FeCo showing the vibrations from the bridging –CN groups in the region of 2000-2300 cm^{-1}.[S5]

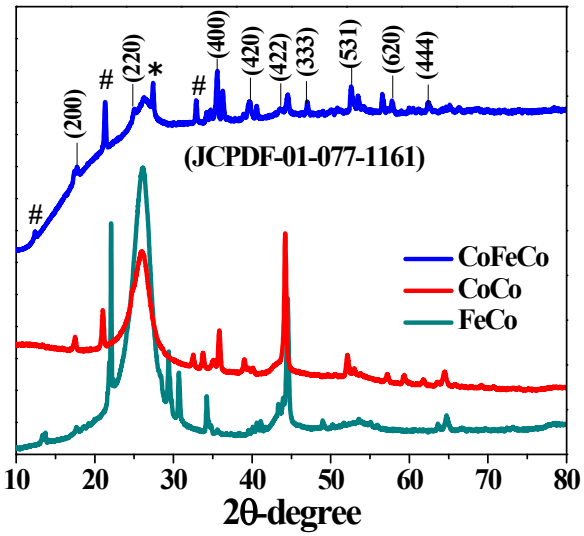

Figure S3. Powder X-ray diffraction patterns of CoFeCo, CoCo and FeCo showing the peaks from the Prussian blue analogue [PBA, cubic, *Fm3m*(225)] with the peaks from metal hydroxide carbonate. The reflections from the PBA are indexed with Miller indices. The peaks corresponded to carbon cloth are * marked. The # marked peaks are generated from the metal hydroxide carbonate template supported on carbon cloth.[S6-S7]

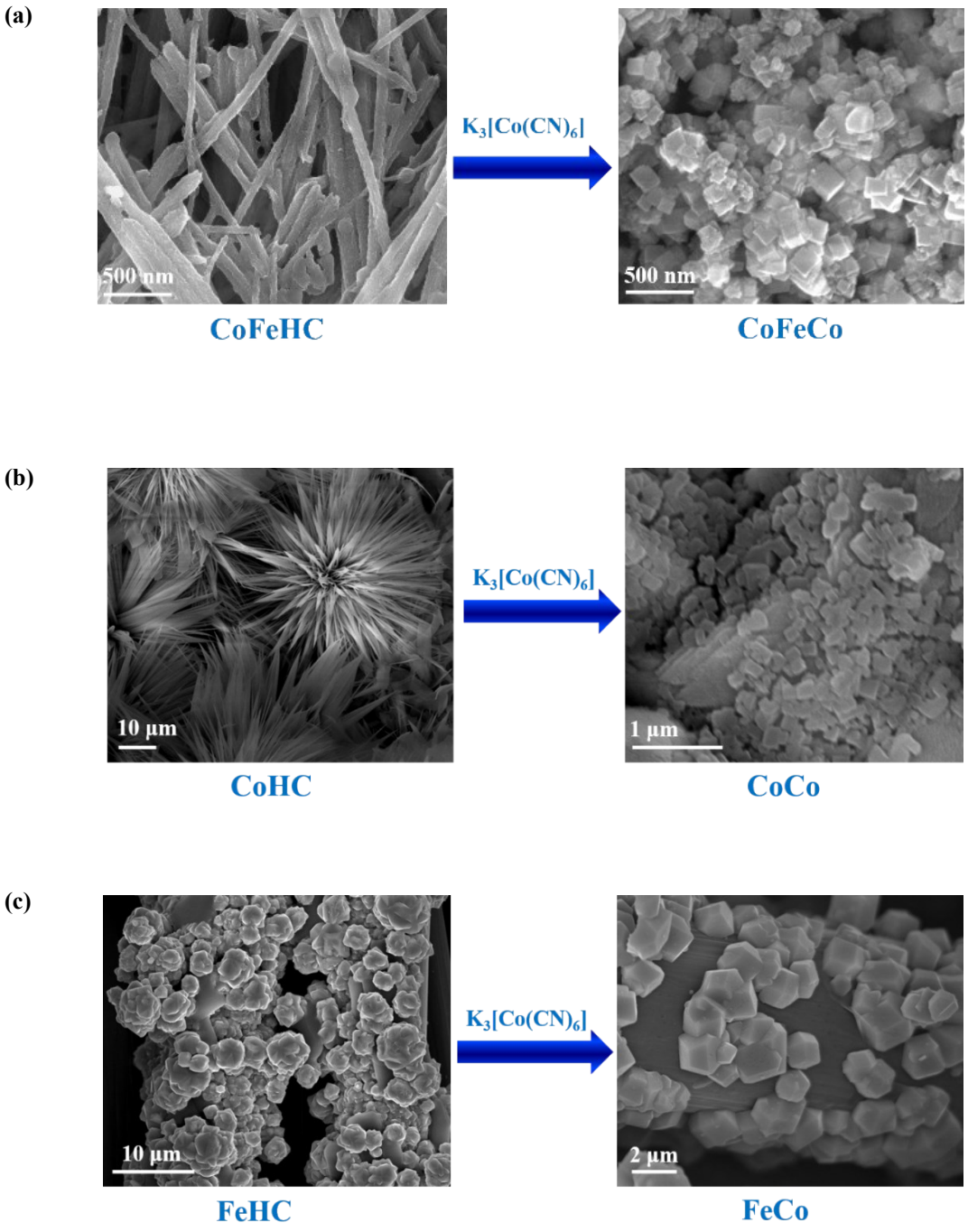

Figure S4. (a) SEM images showing the transformation of CoFeHC nanowire to cubic particles of CoFeCo PBA after the reaction with $K_3[Co(CN)_6]$; (b) SEM images showing the transformation of CoHC nanowire to cubic CoCo particles after the treatment with $K_3[Co(CN)_6]$ and (c) SEM images showing the transformation of FeHC to FeCo after the treatment with $K_3[Co(CN)_6]$.

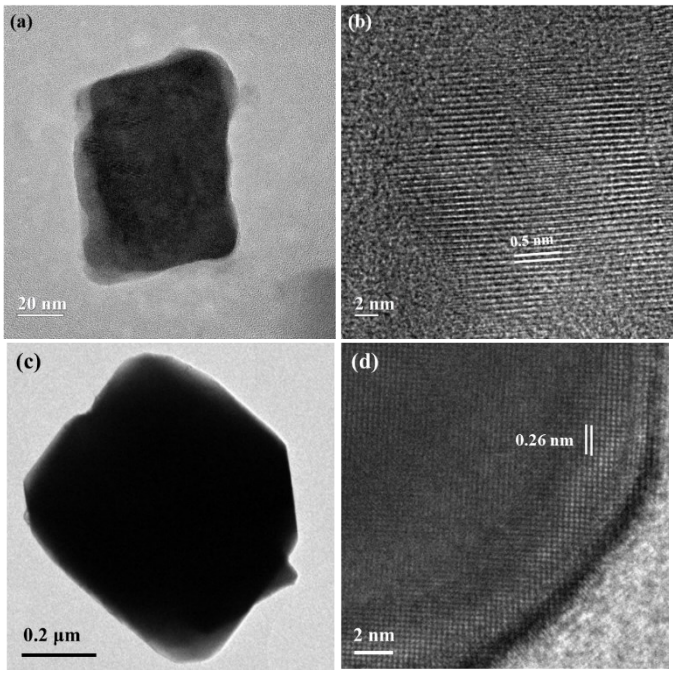

Figure S5. (a) TEM image of fresh CoCo showing the cubic morphology of the particles and (b) HRTEM image of CoCo showing the lattice spacing 0.5 nm corresponding to (200) plane of cubic PBA [space group *Fm3m* (225)]; c) TEM image of fresh FeCo showing the cubic morphology of the particles and (d) HRTEM image of FeCo showing the lattice spacing 0.26 nm corresponding to (400) plane of cubic PBA [space group *Fm3m* (225)].[S8]

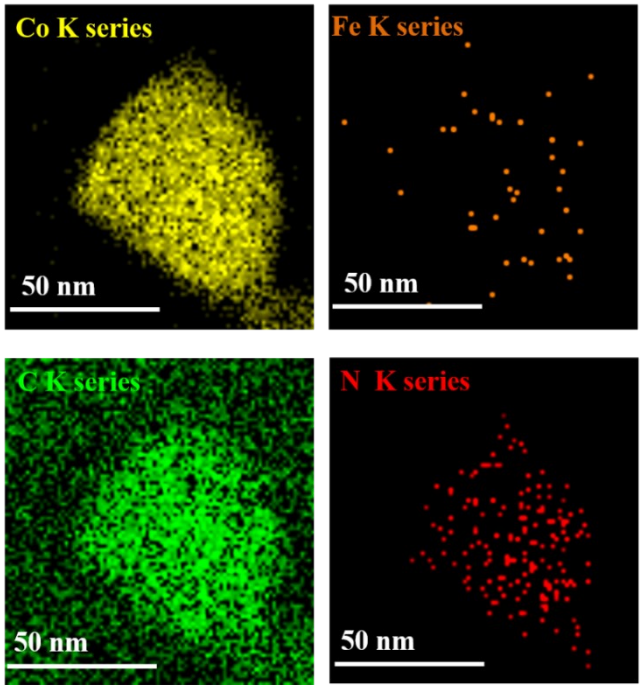

Figure S6. EDX mapping of CoFeCo showing the distribution of the elements Co, Fe, C and N.

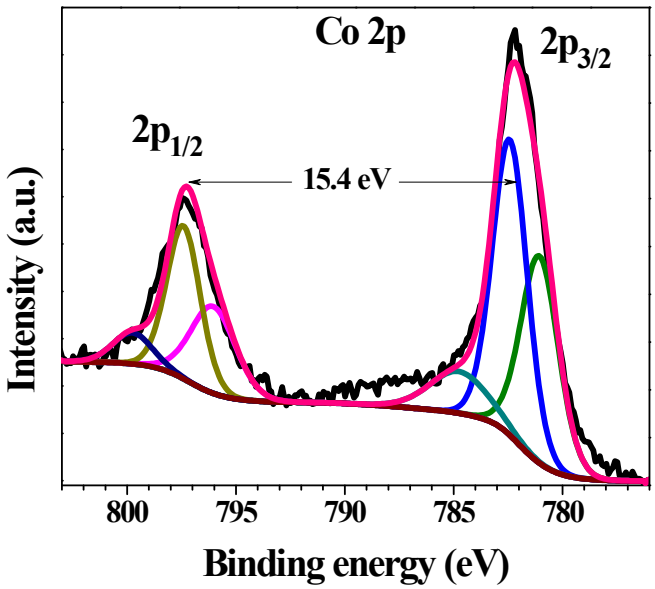

Figure S7. Co 2p X-ray photoelectron spectra of fresh CoFeCo. Co 2p XP-spectrum was fitted into two peaks at binding energies 797.2 eV and 781.8 eV assigned for the Co $2p_{1/2}$ and Co $2p_{3/2}$, respectively. Both the Co $2p_{3/2}$ and Co $2p_{1/2}$ XPS peaks were deconvoluted into Co^{II} and Co^{III} species indicating a mixed valent state of cobalt. The spin-orbit coupling spacing between Co $2p_{3/2}$ and Co $2p_{1/2}$ (15.4 eV) again confirmed the presence of both Co^{II} and Co^{III}.[S9-S11]

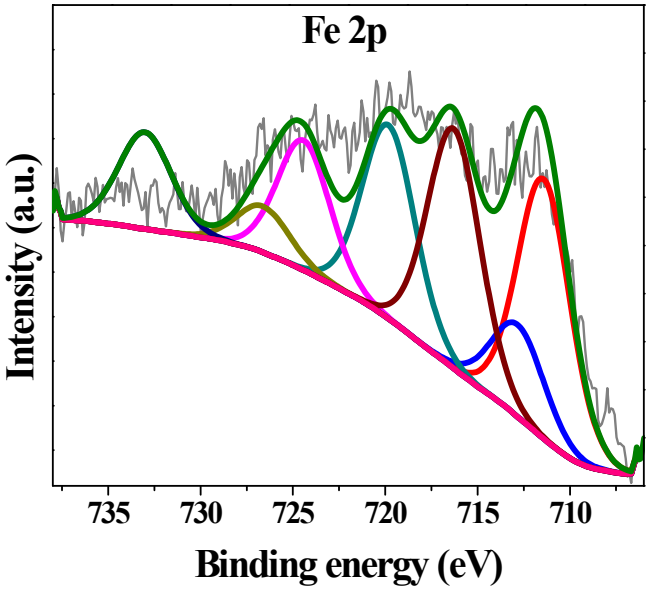

Figure S8. Fe 2p X-ray photoelectron spectra of fresh CoFeCo showing the peaks at binding energy 711.5 eV and 724.5 eV corresponding to $Fe2p_{3/2}$ and $Fe2p_{1/2}$, respectively. The peaks at 711.5 eV and 724.5 eV are assigned for the Fe(III) and the satellite peaks at 716.3 eV and 719.8 eV also indicated the presence of only Fe(III) in the fresh CoFeCo.[S12-S13]

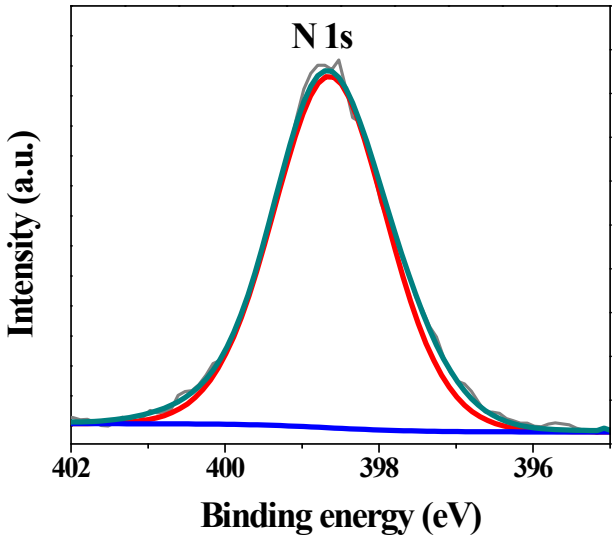

Figure S9. The N 1s XP spectra of fresh CoFeCo representing the peak at binding energy 398.6 eV assigned for the presence of –C≡N moieties of PBA.[S14]

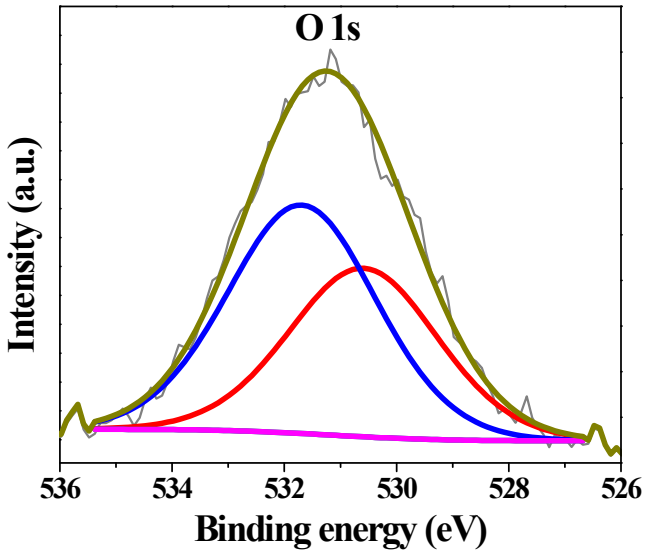

Figure S10. The O 1s XP spectra of fresh CoFeCo deconvoluted in to two peaks at binding energy 530.5 eV and 531.6 eV. The peak at 530.5 eV represents oxygen of the surface –OH groups whereas the peak at 531.6 eV is assigned for the absorbed water molecules.[S15]

Table S2. Comparison of the water oxidation activities of the metal hydroxide carbonate templated Prussian blue analogues (CoFeCo, CoCo and FeCo) with literature reported catalysts in alkaline solution

Catalyst	***Electrolyte***	***Current density (mA cm^{-2})***	***Overpotential (mV)***	***Reference***
Our catalysts				
CoFeCo	*1 M aqueous KOH*	*10*	*220*	*This work*
CoFeCo	*1 M aqueous KOH*	*100*	*290*	*This work*
CoCo	*1 M aqueous KOH*	*10*	*260*	*This work*
FeCo	*1 M aqueous KOH*	*10*	*280*	*This work*
Prussian blue analogue derived catalysts				
NiCo oxide	*1 M aqueous KOH*	*10*	*380*	*S16*
Co_3O_4	*1 M aqueous KOH*	*10*	*370*	*S17*
Ni-P	*1 M aqueous KOH*	*10*	*300*	*S18*
NiCoFeS	*1 M aqueous KOH*	*10*	*320*	*S19*
$(Ni_{0.62}Fe_{0.38})_2P$	*1 M aqueous KOH*	*10*	*290*	*S20*
NiFeP	*1 M aqueous KOH*	*10*	*271*	*S21*
$(NiCo)Se_2$	*1 M aqueous KOH*	*10*	*320*	*S22*
Carbon cloth supported catalysts				
Co-P/NC	*1 M aqueous KOH*	*10*	*330*	*S6*
$CoMoO_4$	*1 M aqueous KOH*	*10*	*290*	*S11*
$CoFe_2O_4$	*1 M aqueous KOH*	*10*	*378*	*S12*
$NiMoP_2$	*1 M aqueous KOH*	*100*	*330*	*S13*
CoP	*1 M aqueous KOH*	*10*	*281*	*S14*
$(Ni,Co)_{0.85}Se$	*1 M aqueous KOH*	*10*	*300*	*S15*
Layered double hydroxide catalysts				
Co_2Fe-LDH	*1 M aqueous KOH*	*10*	*420*	*S23*
ZnCo-LDH	*1 M aqueous KOH*	*10*	*340*	*S24*
NiFe-LDH	*1 M aqueous KOH*	*10*	*259*	*S25*
CoMn-LDH	*1 M aqueous KOH*	*10*	*350*	*S26*
NiFe-LDH	*1 M aqueous KOH*	*10*	*290*	*S27*
CoCr-LDH	*1 M aqueous KOH*	*20*	*400*	*S28*
NiFe-LDH/CNT	*1 M aqueous KOH*	*10*	*300*	*S29*
CoFe-LDH	*1 M aqueous KOH*	*10*	*280*	*S30*
NiFeMo-LDH	*1 M aqueous KOH*	*10*	*280*	*S31*

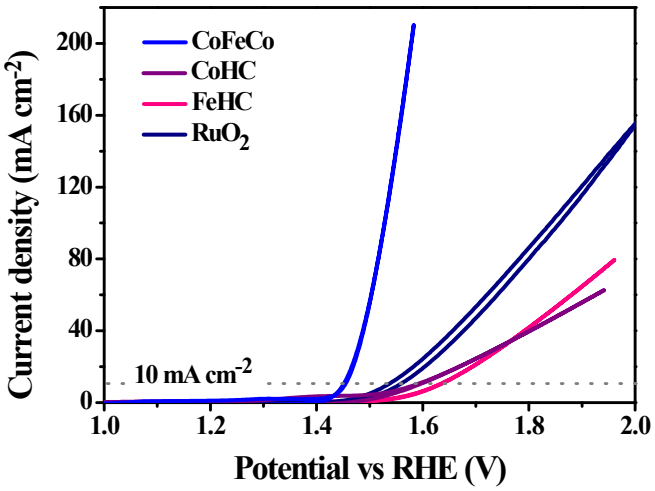

Figure S11. Linear sweep voltammetric profiles for the oxygen evolution reaction of CoFeCo compared with CoHC, FeHC and RuO_2 on carbon cloth showing the improved OER performance for CoFeCo. Reaction conditions: 1.0 M aqueous KOH solution as the electrolyte and 2 mV s^{-1} scan rate. The introduction of Fe in CoHC improved the water oxidation activity for both CoFeHC and corresponding CoFeCo. Improvement in the OER activity by the introduction of redox active second metal (Fe, Mo,Cr etc.) was previously reported by different research groups.[S12,S20,S28,S31] The presence of Fe in the catalyst structure promoted the metal center to attain a high oxidation state in metal-oxyl/hydroxyl intermediates and improved the charge transport.

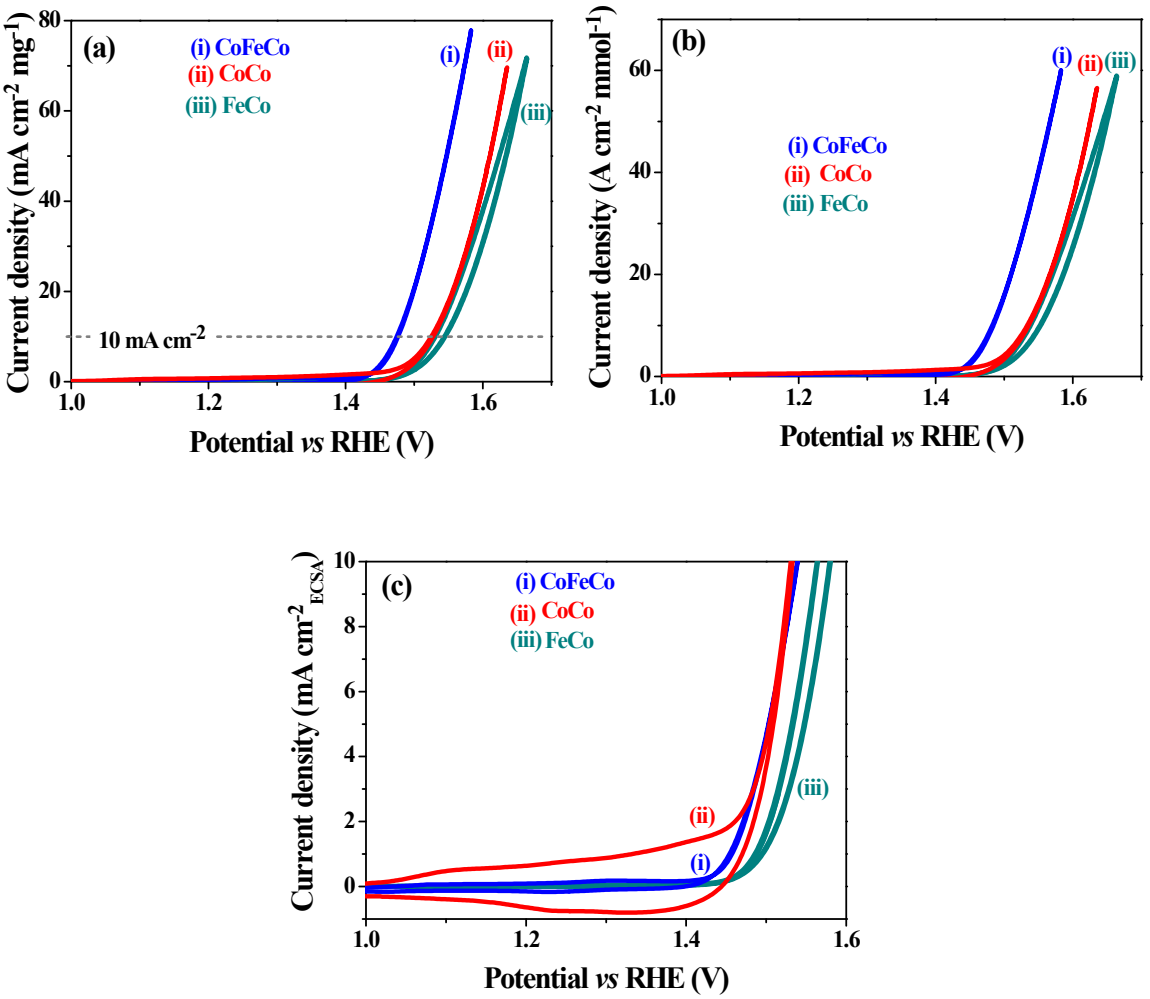

Figure S12. (a) OER catalytic activities of all the synthesized catalysts are normalized against mass loading (all the CV profiles are normalized against per mg of catalyst loading); (b) OER catalytic activities of all the synthesized catalysts are normalized against mmol of catalyst showing the improved OER performance of CoFeCo and (c) OER catalytic activities normalized against ECSA.

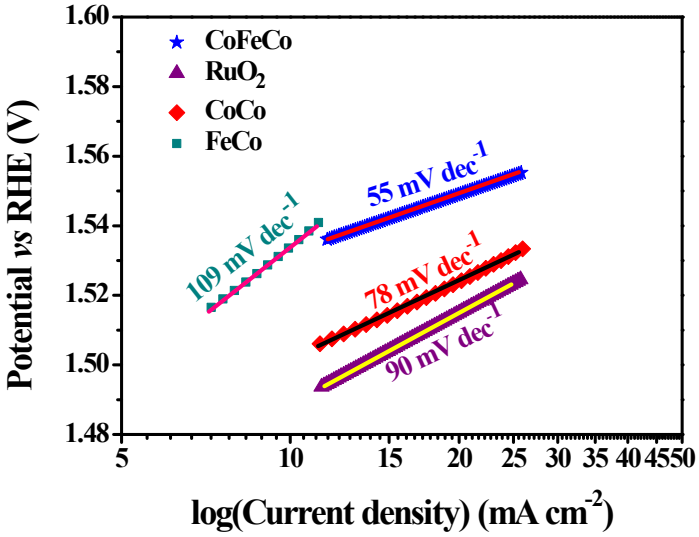

Figure S13. Tafel plots for the oxygen evolution reaction of CoFeCo catalyst compared with FeCo, CoCo and RuO_2 indicating the lowest Tafel slope for CoFeCo catalyst. The lowest Tafel slope suggested the fastest OER kinetics for CoFeCo.

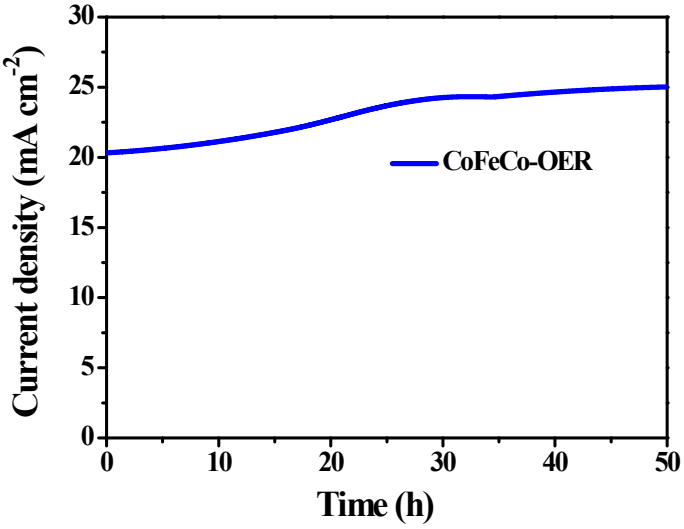

Figure S14. Chronoamperometric alkaline oxygen evolution study with CoFeCo at constant potential of 1.5 V in 1.0 M aqueous KOH solution showing the long term stability for 50 h.

Table S3. Comparison of the hydrogen evolution activities of the metal hydroxide carbonate templated Prussian blue analogues (CoFeCo, CoCo and FeCo) with literature reported catalysts in alkaline solution

Catalyst	*Electrolyte*	*Current density (mA cm^{-2})*	*Overpotential (mV)*	*Reference*
Our catalysts				
CoFeCo	*1 M aqueous KOH*	*10*	*155*	*This work*
CoFeCo	*1 M aqueous KOH*	*100*	*330*	*This work*
CoCo	*1 M aqueous KOH*	*10*	*305*	*This work*
FeCo	*1 M aqueous KOH*	*10*	*215*	*This work*
Prussian blue analogue derived catalysts				
CoNiBO	*1 M aqueous KOH*	*10*	*140*	*S16*
FeP/GA	*1 M aqueous KOH*	*10*	*150*	*S17*
NiCoP	*1 M aqueous KOH*	*10*	*150*	*S18*
NiFe/CN	*1 M aqueous KOH*	*10*	*281*	*S19*
NC-NiFeO$_x$@NiFe-P	*1 M aqueous KOH*	*10*	*237*	*S20*
NiFeP	*1 M aqueous KOH*	*10*	*182*	*S21*
Co-FeN$_x$	*1 M aqueous KOH*	*10*	*183*	*S22*
Carbon cloth supported catalysts				
Co-P/NC	*1 M aqueous KOH*	*10*	*171*	*S6*
CoS$_2$	*1 M aqueous KOH*	*10*	*193*	*S32*
CoSe$_2$	*1 M aqueous KOH*	*10*	*113*	*S33*
NiMoP$_2$	*1 M aqueous KOH*	*100*	*199*	*S13*
CoP	*1 M aqueous KOH*	*10*	*95*	*S14*
NiCoN	*1 M aqueous KOH*	*10*	*145*	*S34*
Layered double hydroxide catalysts				
CoFe-LDH	*1 M aqueous KOH*	*50*	*273*	*S36*
NiFeV-LDH	*1 M aqueous KOH*	*10*	*125*	*S37*
NiFeMn-LDH	*1 M aqueous KOH*	*10*	*110*	*S38*
NiFe-LDH/NiSe	*1 M aqueous KOH*	*10*	*276*	*S39*

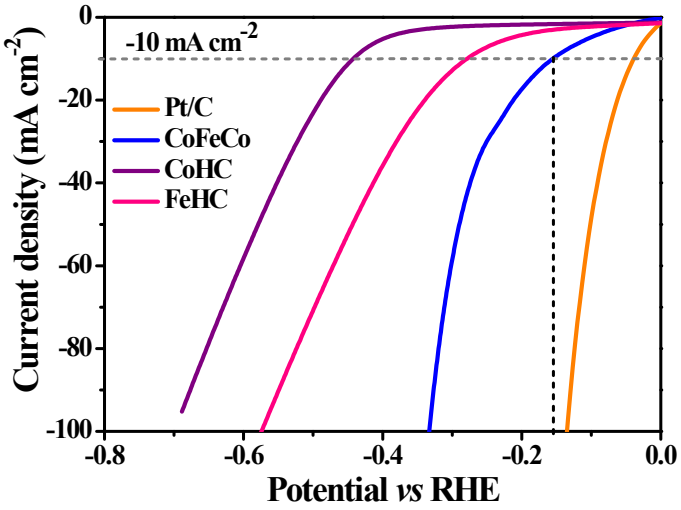

Figure S15. Linear sweep voltammetric profiles for the hydrogen evolution reaction with CoFeCo compared with 20% Pt/C on carbon cloth, CoHC and FeHC. Reaction conditions: 1.0 M aqueous KOH solution as the electrolyte and 2 mV s^{-1} scan rate.

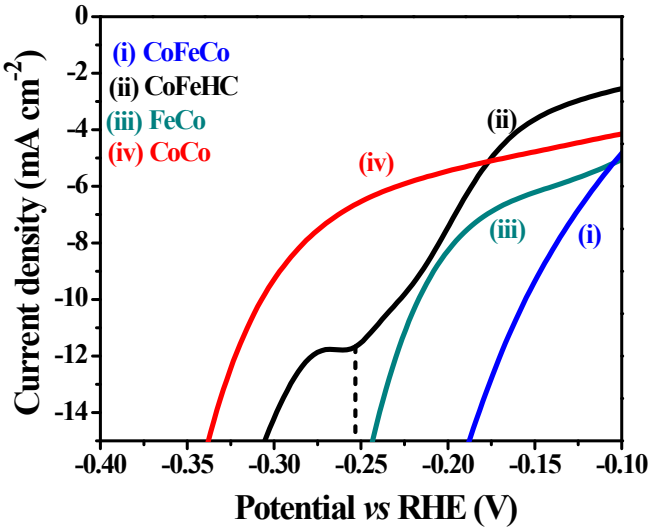

Figure S16. LSV profile for hydrogen evolution reaction of CoFeCo, CoCo, FeCo and CoFeHC. A prominent cathodic peak was observed for CoFeHC at -254 mV vs RHE attributed to the reduction of Fe(III) to Fe(0)/Fe(I) species.[S40]

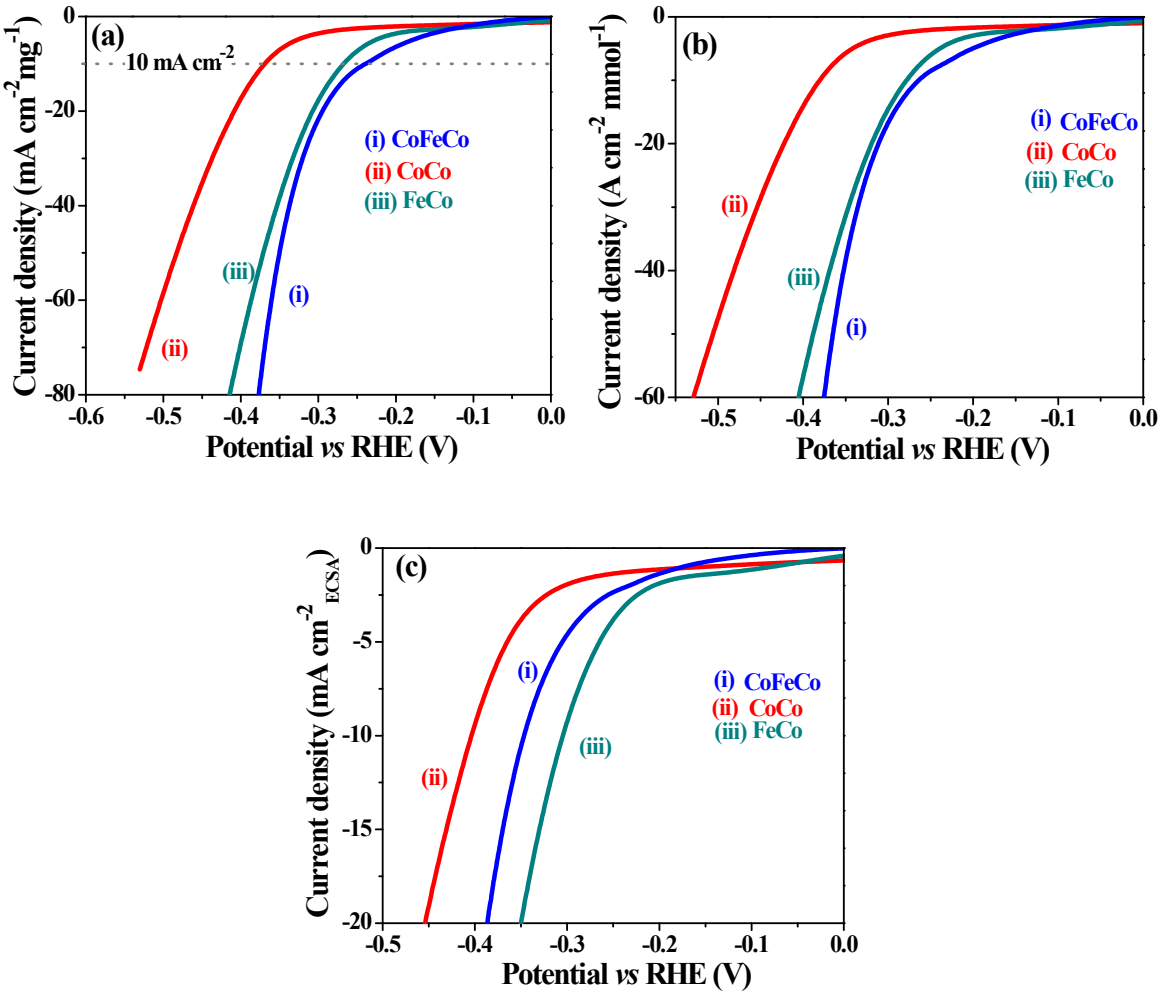

Figure S17. (a) HER catalytic activities of all the synthesized catalysts are normalized against mass loading (all the LSV profiles are normalized against per mg of the catalyst loading); (b) HER catalytic activities of all the synthesized catalysts are normalized against mmol of catalyst showing the improved HER performance of CoFeCo and (c) HER catalytic activities normalized against ECSA. It should be mentioned here that the HER activity of CoCo was a poor and drastic improvement in HER activity was observed when Fe was introduced in the PBA system. Fe incorporation results in the optimization of the free energy and increases the number of active sites for the adsorption of protons on the catalytic surface.

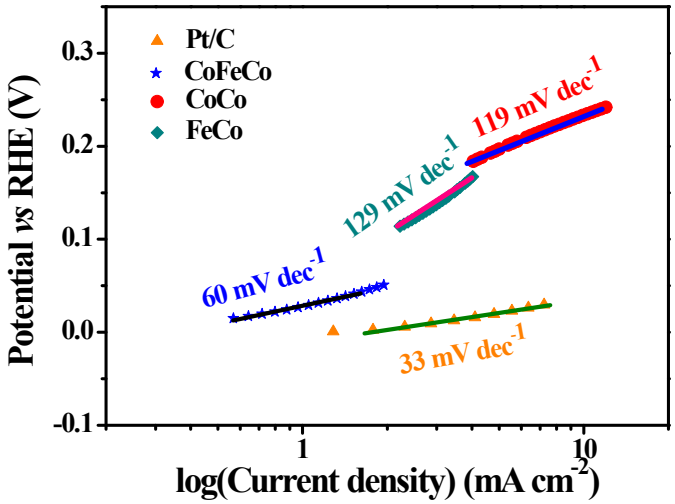

Figure S18. Tafel plots for the hydrogen evolution reaction of CoFeCo catalyst compared with FeCo, CoCo and Pt/C indicating the lowest Tafel slope for CoFeCo among the synthesized catalyst. The lowest Tafel slope suggested the fastest HER kinetics for CoFeCo.

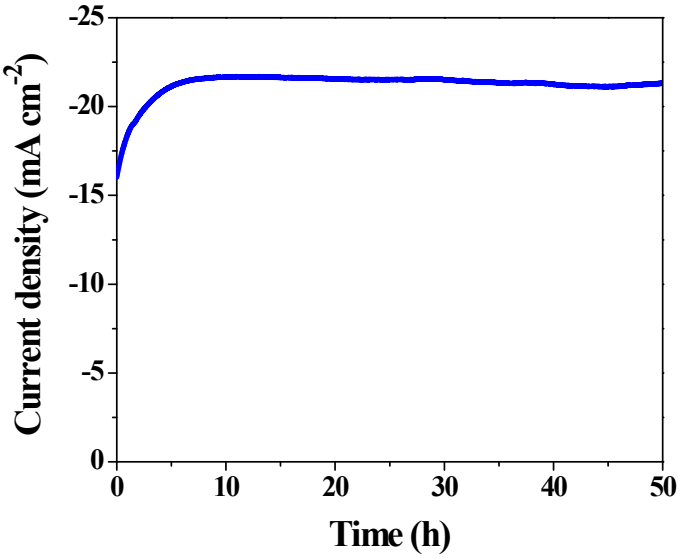

Figure S19. Chronoamperometric hydrogen evolution reaction with CoFeCo at -0.20 V vs RHE showing the long term stability of the catalyst system in 1.0 M aqueous KOH solution.

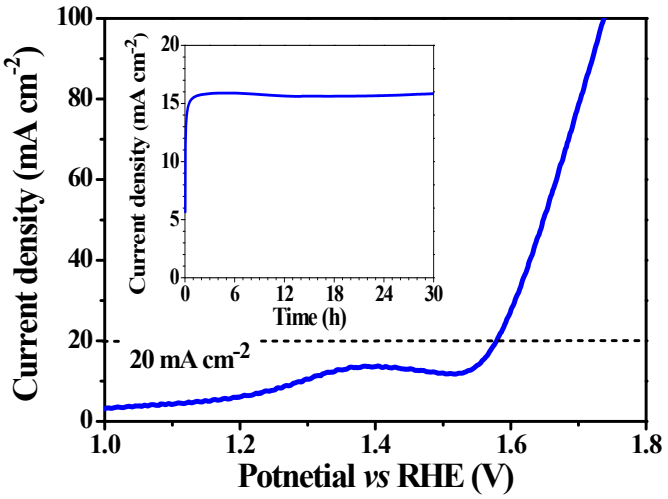

Figure S20. Linear sweep voltammetric profile for the overall water splitting of CoFeCo demonstrating 20 mA cm^{-2} current density at only cell voltage 1.58 V (Inset: chronoamperometric stability test showing the enhanced stability of CoFeCo for 30 h).

Calculation of Faradaic efficiency for overall water splitting

The Faradaic efficiency (FE) of CoFeCo electrocatalyst towards overall water splitting was measured with a two-electrode configuration in 1M aqueous electrolyte. The CoFeCo was used both as an anode and a cathode in a closed single-compartment electrochemical cell. The electrolyte and cell were first degassed with argon (Ar) for 1 hour under constant stirring. The catalysts were first activated by applying a constant current density of 10 mA cm^{-2} and subsequently, applied for FE measurement for a time period of 150 seconds. At the end of electrolysis, the gaseous samples were drawn from the headspace by a gas-tight syringe and analyzed by a GC calibrated for H_2 and O_2. Each injection was repeated at least three times, and the average value is presented. Our measurements also considered the initial quantity of trace O_2 from the air (if present) to determine the amount of produced O_2. We performed a blank measurement by bubbling the electrolyte with Ar for 1 h to displace any gas dissolved in the electrolyte solution as well as at the headspace and measured the resulting atmosphere by gas chromatography (GC). Then, the amount of trace O_2 is subtracted from the volume of produced oxygen obtained from the GC.

The FE is calculated based on:

$$FE(H_2, \%) = \frac{V_{H_2} \times 2 \times F}{V_m \times j \times t} \times 100\%$$

$$FE(O_2, \%) = \frac{V_{O_2} \times 4 \times F}{V_m \times j \times t} \times 100\%$$

V_{H2} and V_{O2} are the evolved volume of hydrogen and oxygen, F is the Faraday constant (96485.33289 C mol^{-1}), V_m is the molar volume of the gas, j is the current density (10 mA cm^{-2}) and t is the time of electrolysis (150 s).

Table S4. Calculation of Faradaic efficiency for CoFeCo.

Catalysts	j (mA cm^{-2})	t (s)	V_{H_2} (mL)	V_{O_2} (mL)	V_{H_2}/V_{O_2}	FE (H_2, %)	FE (O_2, %)
CoFeCo	10	150	0.18 ± 0.04	0.09 ± 0.02	1.99 ± 0.06	95 ± 1%	95 ± 3%

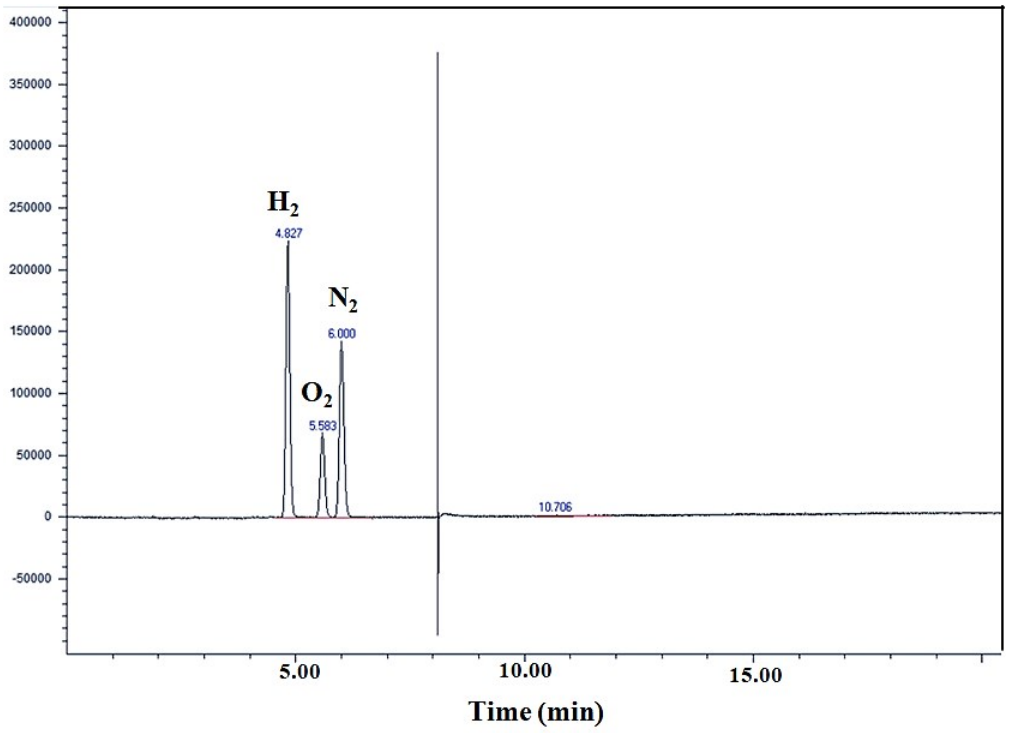

Figure S21. GC studies for the determination of the produced H_2 and O_2 during electrochemical overall water splitting with CoFeCo||CoFeCo catalyst system.

Table S5. Comparison of the overall water splitting activities of the metal hydroxide carbonate templated Prussian blue analogues (CoFeCo, CoCo and FeCo) with literature reported catalysts in alkaline solution

Catalyst	***Electrolyte***	***Current density (mA cm^{-2})***	***Cell Voltage (V)***	***Reference***
Our catalysts				
CoFeCo	*1 M aqueous KOH*	*20*	*1.58*	*This work*
CoFeCo	*1 M aqueous KOH*	*50*	*1.64*	*This work*
Prussian blue analogue derived catalysts				
NC-NiFeO$_x$@NiFe-P	*1 M aqueous KOH*	*10*	*1.59*	*S41*
CoFeSeP	*1 M aqueous KOH*	*10*	*1.59*	*S42*
Fe-CoP	*1 M aqueous KOH*	*10*	*1.49*	*S43*
CoNiPS$_3$/C	*1 M aqueous KOH*	*10*	*1.62*	*S44*
FeCoNi@NC	*1 M aqueous KOH*	*10*	*1.68*	*S45*
CoS$_2$@CC	*1 M aqueous KOH*	*10*	*1.62*	*S46*
NiFe-oxide	*1 M aqueous KOH*	*10*	*1.67*	*S47*
Carbon cloth supported catalysts				
Co-P/NC	*1 M aqueous KOH*	*10*	*1.70*	*S6*
CoS$_2$	*1 M aqueous KOH*	*10*	*1.62*	*S32*
Co$_3$S$_4$	*1 M aqueous KOH*	*10*	*1.55*	*S35*
NiMoP$_2$	*1 M aqueous KOH*	*10*	*1.67*	*S13*
CoP	*1 M aqueous KOH*	*10*	*1.61*	*S14*
NiCoN	*1 M aqueous KOH*	*10*	*1.68*	*S34*

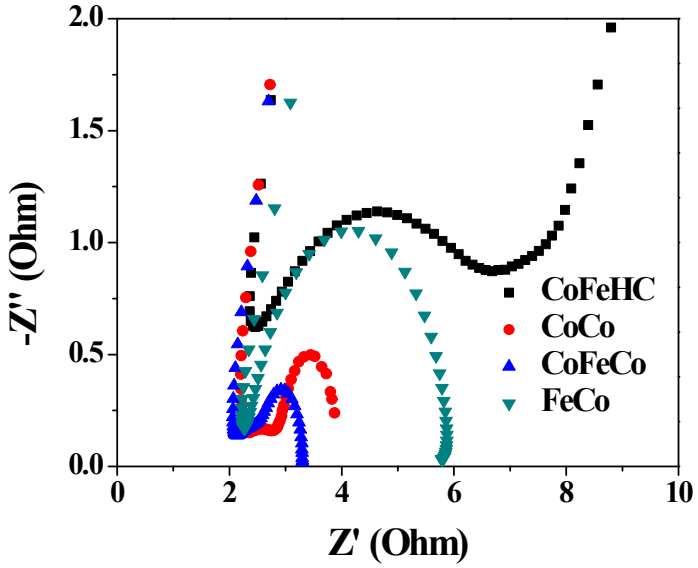

Figure S22. Nyquist plots for the carbon cloth supported templated PBAs-CoFeCo, CoCo and FeCo obtained from electrochemical impedance spectroscopic (EIS) measurements showing showed lower charge transfer resistance for CoFeCo catalyst. The spectra were collected with an anodic polarization potential of 1.5 V vs RHE. The improved electrochemical performance of the templated CoFeCo can be elucidated by the formation of an integrated system that unifies the factors like availability of a large number of active sites and improved electron transport with strong catalyst-support interaction.

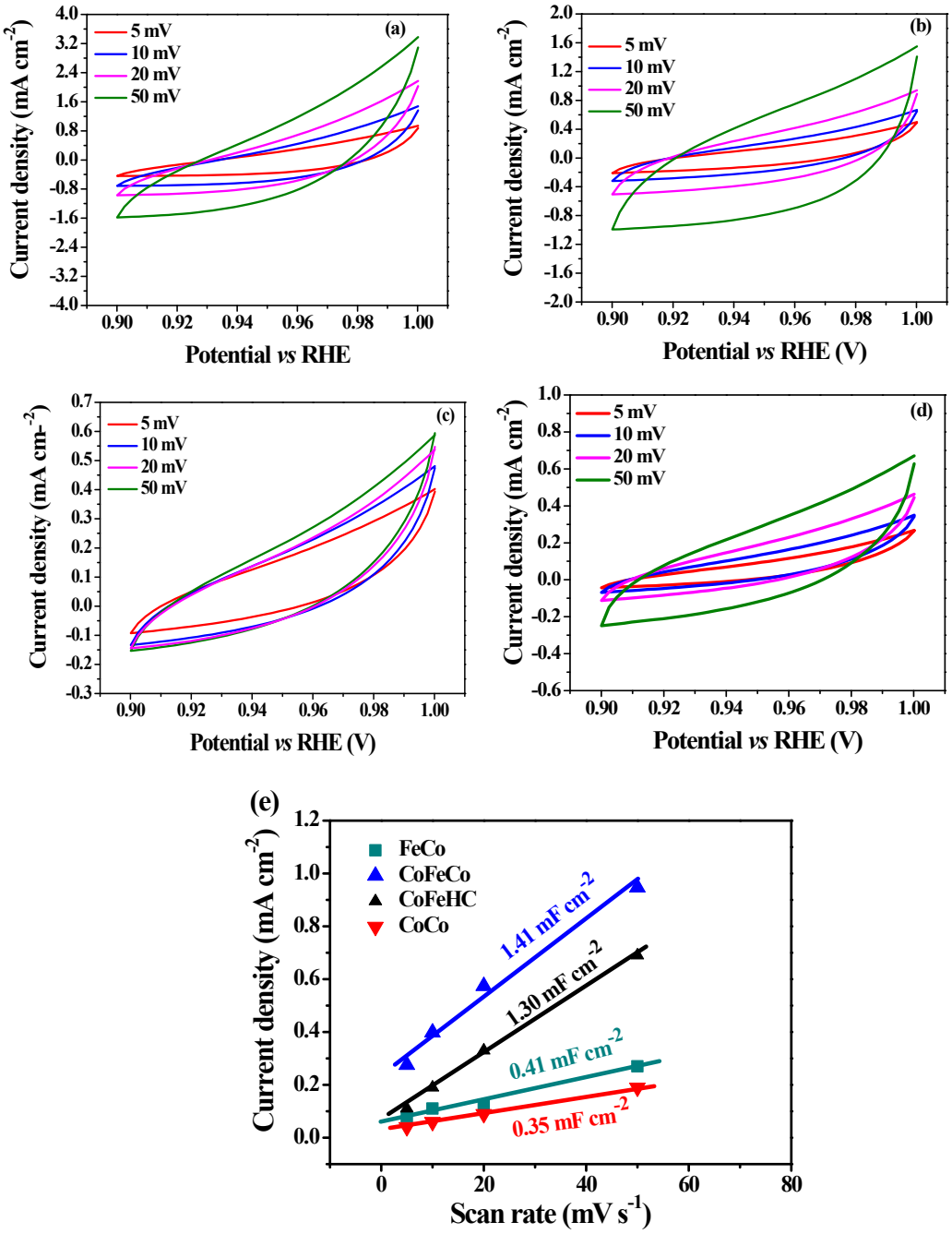

Figure S23. Electrochemical capacitance current of a) CoFeCo; b) CoFeHC; c) FeCo and d) CoCo in the non-Faradaic potential range of 0.96 V to 1.06 V vs RHE with variation in scan rate (5, 10, 20, 50 mV/s) in 1.0 M aqueous KOH solution. (e) Determination of double-layer capacitance (C_{dl}) of CoFeCo, CoCo, FeCo and CoFeHC by plotting (difference in current density)/2 against scan rate.

The specific capacitance of 1 cm^2 flat surface area is in the range of 20-60 μF cm^{-2}-which can be averaged to 40 μF cm^{-2}.[S32-S34] The C_{dl} value was converted to the electrochemical surface area (ECSA) using the equation:

ECSA = C_{dl} of catalyst in mF/0.04 mF cm^{-2}

ECSA of CoFeCo = 1.41/0.04 = **35.25 cm^2/2.9 mg = 12.15 cm^2/mg**

ECSA of CoFeHC = 1.30/0.04 = **32.5 cm^2/2.7 mg = 12.0 cm^2/mg**

ECSA of FeCo = 0.41/0.04 = **10.25 cm^2/2.3 mg = 4.45 cm^2/mg**

ECSA of CoCo = 0.35/0.04 = **8.75 cm^2/2.6 mg = 3.36 cm^2/mg**

Characterizations after Electrochemical Transformation

Recently, the electrochemical transformation of metal organic frameworks into layered double hydroxide nanosheets was reported during alkaline water splitting. NiFe-MOF, NiFe-MOF@NF, CoNi-MOF@CF and NiFeCo-MOF@NF were demonstrated to form ultrathin Ni hydroxide-(oxy)hydroxide nanosheets during alkaline water splitting.[S48] In fact, surface activation and structural transformation of most of the first-row transition metal based catalysts into the metal hydroxide-(oxy)hydroxide structure was detected during the alkaline water oxidation.[S48-S49] Therefore, we have performed detail spectroscopic and microscopic studies of CoFeCo after OER-CA and HER-CA measurements (24 h). The Fe leaching during the electrochemical transformation of the catalyst in alkaline water oxidation was reported by other research groups.[S50] The 23% Fe-leaching of iron in NiFe-MOF was reported by Duan et al. after CA-measurement.[S50a] Speck et al. also detected only 17% of iron after CA measurement of FeNiO during the water oxidation.[S50b] The leaching of iron during CA measurement resulted in the formation of the cationic vacancies and exposed active sites generating structural defects.[S50-S51] The presence of a small amount of Fe in the catalyst structure promoted metal centers to attain a high oxidation state in M-oxo/oxyl intermediate resulting in the improved charge transport and exposed inner active sites.[S50-S51]

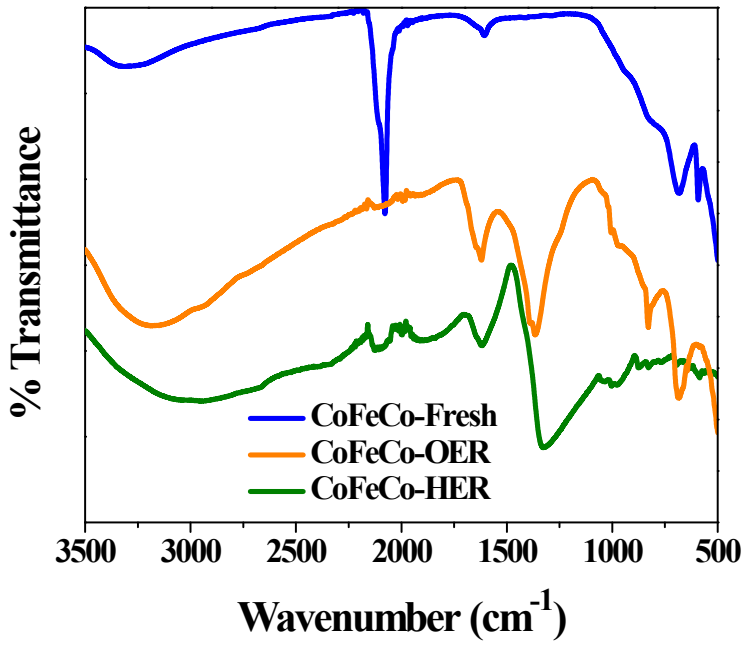

Figure S24. FTIR spectrum of CoFeCo after 24 h of continuous chronoamperometric measurements in 1.0 M aqueous KOH solution showing the disappearance of –CN peaks of PBA.

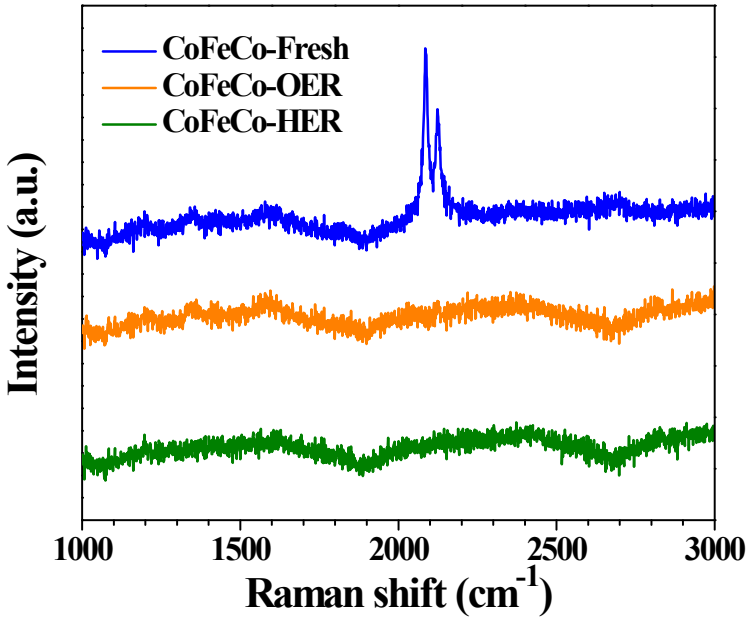

Figure S25. Raman spectrum of CoFeCo after 24 h of continuous chronoamperometric measurements in 1.0 M aqueous KOH solution showing the disappearance of the peak of –CN after HER and OER.

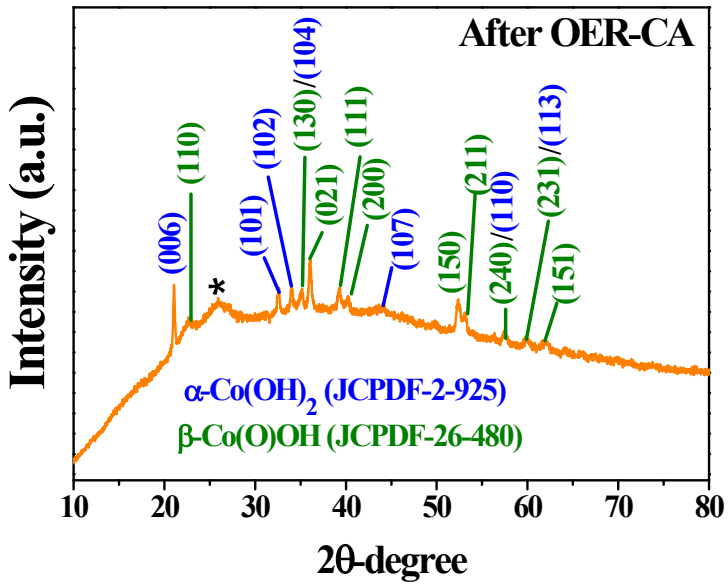

Figure S26. PXRD pattern of electrochemically transformed CoFeCo after 24 h of OER-CA. PXRD pattern was well indexed for the mixed phase α-$Co(OH)_2$ and β-Co(O)OH matching with JCPDF-2-925 and JCPDF-26-480, respectively.

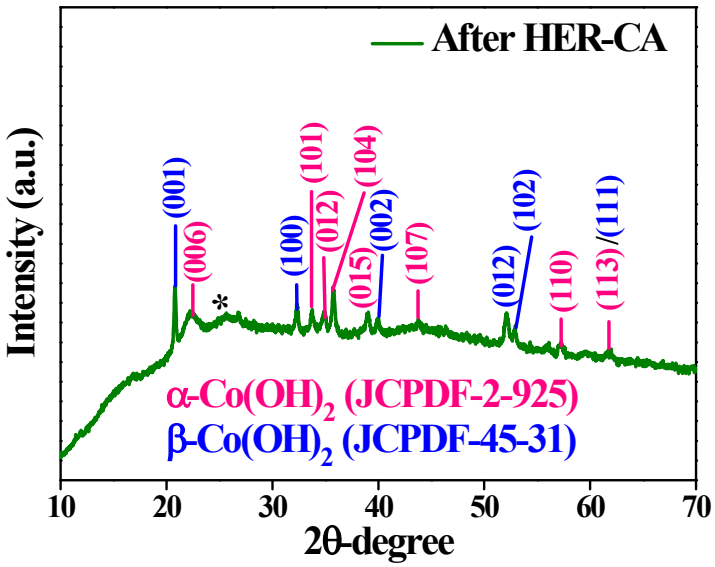

Figure S27. PXRD pattern of electrochemically transformed CoFeCo after 24 h of HER-CA. PXRD pattern was well indexed for the mixed phase α-$Co(OH)_2$ and β-$Co(OH)_2$ matching with JCPDF-2-925 and JCPDF-45-31, respectively.

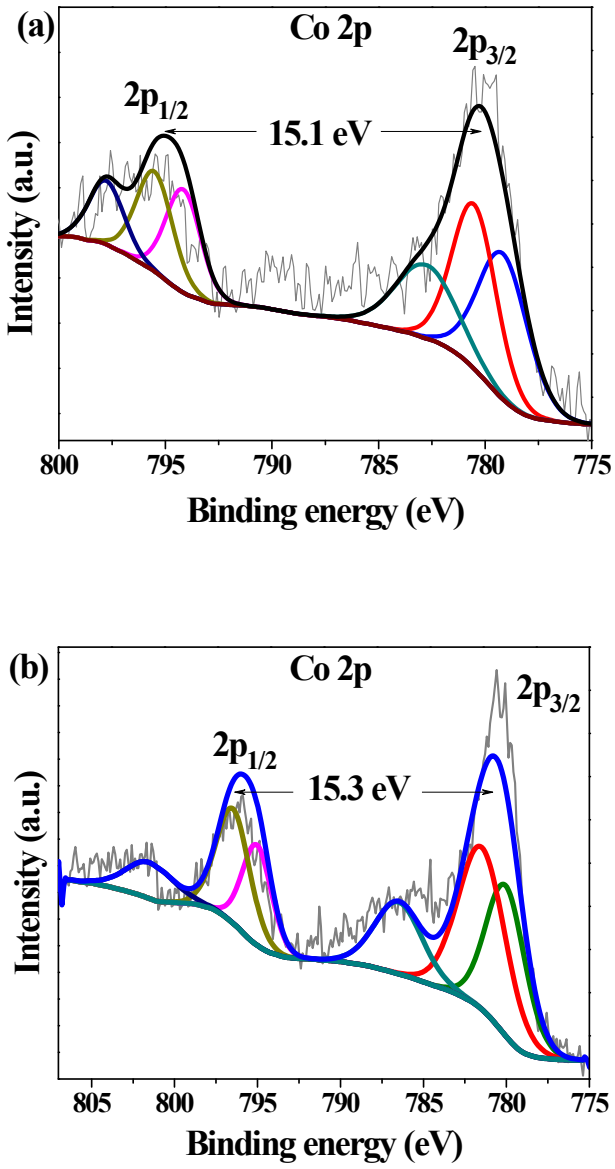

Figure S28. Co 2p X-ray photoelectron spectra of (a) CoFeCo after 24 h of continuous OER-CA at -1.5 V and (b) CoFeCo after 24 h of continuous HER under chronoamperometric conditions at constant potential of -0.20 V in 1.0 M aqueous KOH solution. After CA OER, Co $2p_{3/2}$ and $2p_{1/2}$ spin-orbit coupling value is determined to be 15.1 eV explaining the oxidation of some of the Co(II) centers to Co(III). After CA HER, the Co $2p_{3/2}$ and $2p_{1/2}$ spin-orbit spacing was calculated to be 15.3 eV showing the presence of mixed valent Co(II) a Co(III) and substantial change in the peak positions was also observed.[S52-S53]

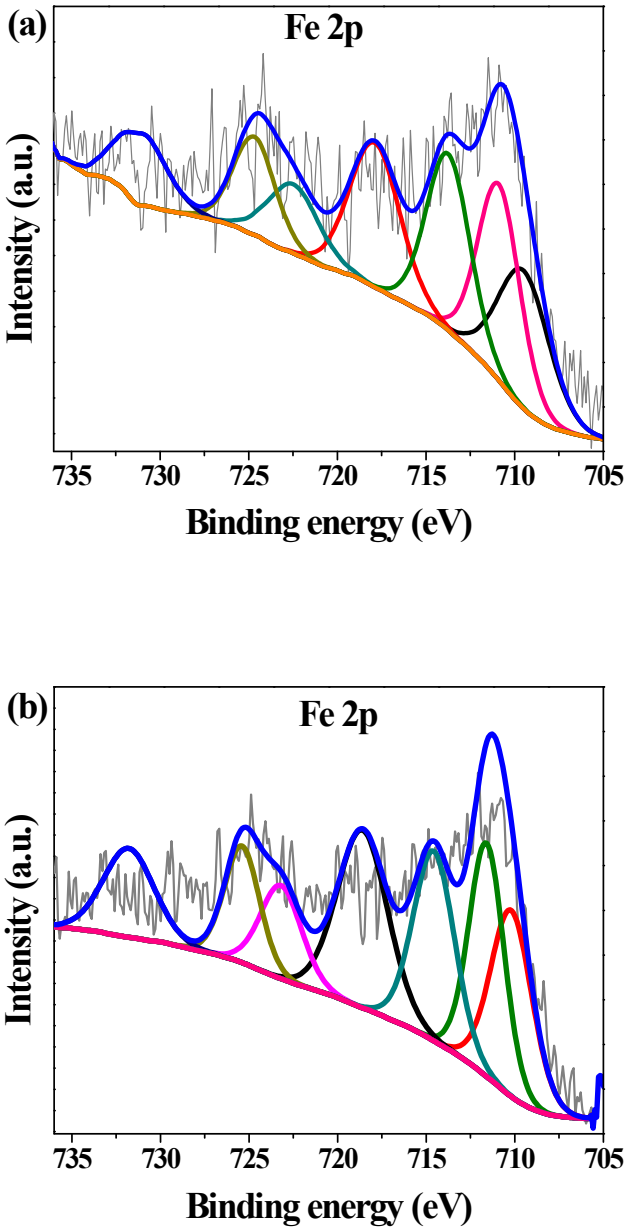

Figure S29. Fe 2p X-ray photoelectron spectra of (a) CoFeCo after 24 h of continuous OER-CA at 1.5 V and (b) CoFeCo after 24 h of continuous HER under chronoamperometric conditions at constant potential of -0.20 V in 1.0 M aqueous KOH solution. After OER-CA, new peaks for Fe(II) (709.6 eV and 722.5 eV) were produced along with the peaks from Fe(III) (711.1 eV and 724.7 eV). After HER-CA, peaks for Fe(III) were observed at 711.1 eV and 724.7 eV whereas Fe(II) peaks were assigned at the binding energies of 709.4 eV and 722.8 eV.[S54-S55] This mixed valency of Fe can be explained by the formation of a layered hydroxide structure.

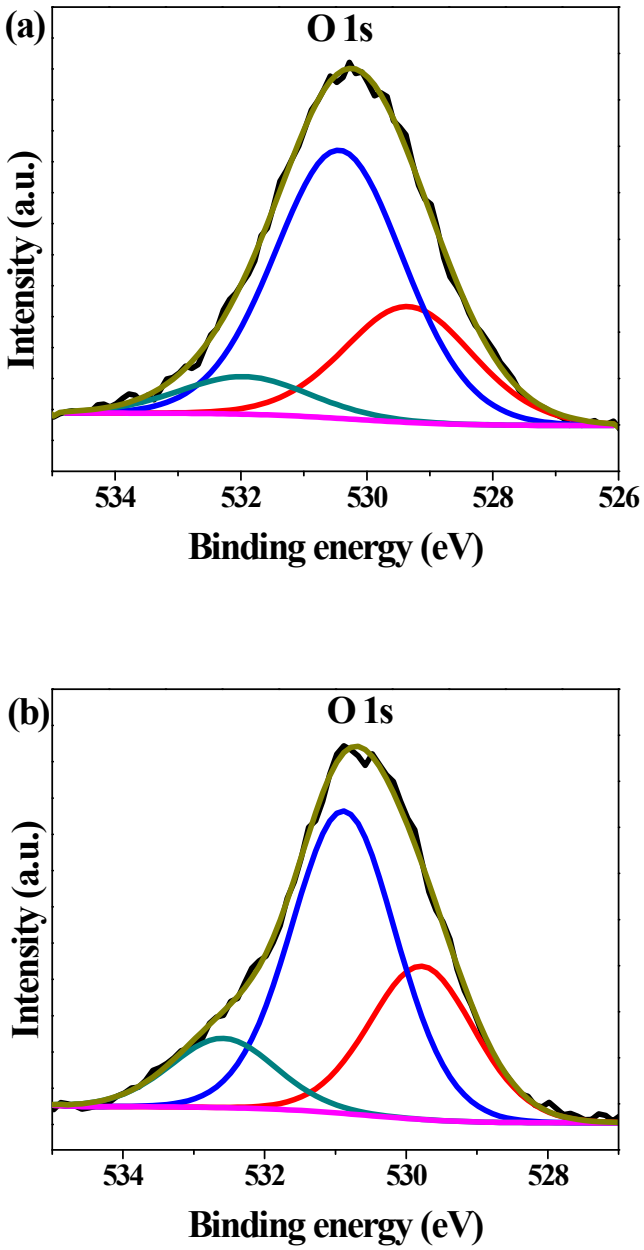

Figure S30. The O 1s XPS spectra of (a) CoFeCo after 24 h of continuous OER-CA at 1.5 V and (b) CoFeCo after 24 h of continuous HER under chronoamperometric conditions at constant potential of -0.20 V in 1.0 M aqueous KOH solution. After OER CA, the peak at binding energy 529.4 eV was assigned to metal–oxygen bonds in the layered metal hydroxide or oxyhydroxide. After HER CA, the peaks at binding energy 529.7 eV was assigned to metal–oxygen bonds.[S54-S55]

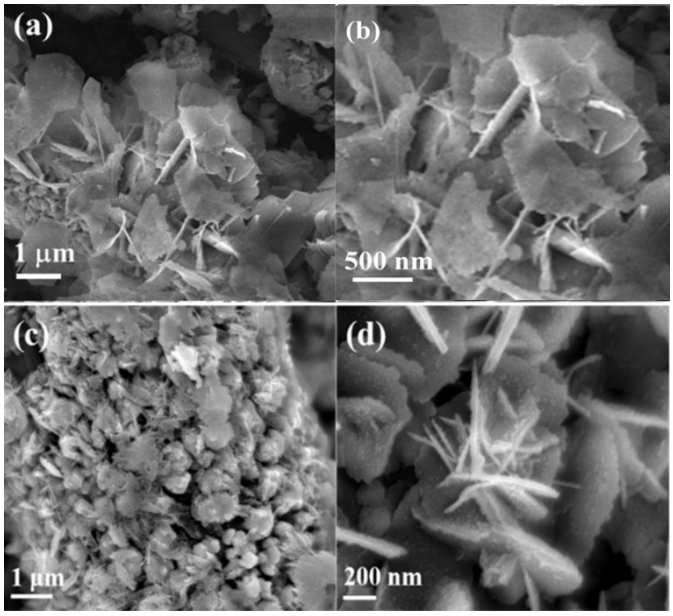

Figure S31. (a-b) SEM images of CoFeCo after continuous oxygen evolution for 24 h at constant potential of 1.5 V under chronoamperometric conditions. (**c-d**) SEM images of CoFeCo after continuous hydrogen evolution for 24 h at constant potential of -0.20 V under chronoamperometric conditions. Complete destruction of the cubic morphology to form layered oxyhydroxide and hydroxide is visible from the SEM studies.

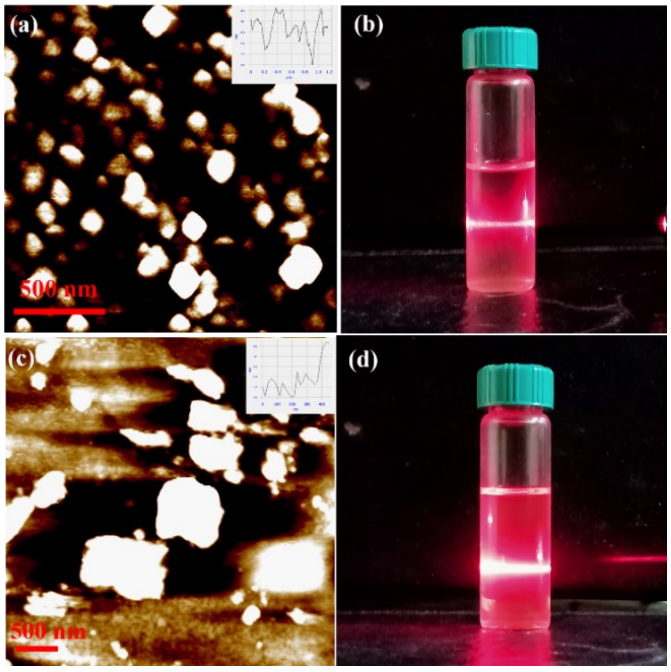

Figure S32. a) Atomic force microscopic topography image of CoFeCo after 24 h continuous OER-CA measurements showing the thickness of 6 nm for the ultrathin nanosheets (inset height profile); b) Tyndall effect CoFeCo after 24 h continuous OER-CA measurements indicates ultrathin nanosheets morphology; c) AFM topography image of CoFeCo after 24 h continuous HER-CA showing the thickness of 3 nm for ultrathin nanosheets (inset height profile) and d) Tyndall effect after HER-CA indicates ultrathin nanosheets morphology.

References

S1 R. Ge, H. Du, K. Tao, Q. Zhang and L. Chen, *ACS Appl. Mater. Interfaces,* 2017, **9**, 15383-15387.

S2 Y. Zhao, H. Ma, S. Huang, X. Zhang, M. Xia, Y. Tang and Z. Ma, *ACS Appl. Mater. Interfaces,* 2016, **8**, 22997-23005.

S3 S. Bao, W. Qin, Q. Wu, G. Liang, F. Zhua and Q. Wu, *Dalton Trans.,* 2013, **42**, 5242-5246.

S4 a) Y. Yin, Q. Li, S. Ma, H. Liu, B. Dong, J. Yang and D. Liu, *Anal. Chem.,* 2017, **89**, 1551-1557; b) Q. Wang, N. Wang, S. He, J. Zhao, J. Fang and W. Shen, *Dalton Trans.,* 2015, **44**, 12878-12883; c) H. Guo, T. Li, W. Chen, L. Liu, X. Yang, Y. Wang and Y. Guo, *Nanoscale,* 2014, **6**, 15168-15174.

S5 a) J. Yang, X. Zhang, Z. Xu and J. Huang, J. Chen, *J. Electroanalytical Chem.,* 2017, **788**, 54-60; b) Y. Yin, Q. Li, S. Ma, H. Liu, B. Dong, J. Yang and D. Liu, *Anal. Chem.,* 2017, **89**, 1551-1557.

S6 a) X. Liu, J. Dong, B. You and Y. Sun, *RSC Adv.,* 2016, **6**, 73336-73342; b) Y. Shen, S. G. Guo, F. Du, X. B. Yuan, Y. Zhang, J. Hu, Q. Shen and W. Luo, A. Alsaedi, T. Hayat, G. Wen, G. L. Li, Y. Zhou and Z. Zou, *Nanoscale,* 2019, **11**, 11765-11773; c) Y. Zhao, H. Ma, S. Huang, X. Zhang, M. Xia, Y. Tang and Z. Ma*, ACS Appl. Mater. Interfaces,* 2016, **8**, 22997-23005.

S7 a) Yang, M. Zhou, W. Guo, X. Cui, Y. Li, F. Liu, P. Xiao and Y. Zhang, *Electrochim. Acta,* 2015, **174**, 246-253; b) R. Chen, Y. Huang, M. Xie, Q. Zhang, X. Zhang, L. Li and F. Wu, *ACS Appl. Mater. Interfaces,* 2016, **8**, 16078-16086.

S8 Y. Feng, X. Wang, P. Dong, J. Li, L. Feng, J. Huang, L. Cao, L. Feng, K. Kajiyoshi and C. Wang, *Sci. Rep.,* 2019, **9**, 15965.

S9 Z. Wang, J. Li, X. Tian, X. Wang, Y. Yu, K. A. Owusu, L. He and L. Mai, *ACS Appl. Mater. Interfaces,* 2016, **8**, 19386-19392.

S10 N. Cheng, Q. Liu, J. Tian, X. Sun, Y. He, S. Zhai and A. M. Asiri, *Intl. J. Hydrogen Energy,* 2015, **40**, 9866-9871.

S11 J. Meng, J. Fu, X. Yang, M. Wei, S. Liang, H. Zang, H. Tan, Y. Wang and Y. Li, *Inorg. Chem. Front.,* DOI:10.1039/C7QI00435D.

S12 A. Kargar, S. Yavuz, T. K. Kim, C. Liu, C. Kuru, C. S. Rustomji, S. Jin and P. R. Bandaru, *ACS Appl. Mater. Interfaces*, 2015, 7, 17851-17856.

S13 X. Wang, H. Chen, Y. Xu, J. Liao, B. Chen, H. Rao, D. Kuang and C. Su . *J. Mater. Chem., A* 2017, **5**, 7191-7199.

S14 P. Wang, F. Song, R. Amal, Y. H. Ng and X. Hu, *ChemSusChem,* 2016, **9**, 472-477.

S15 C. Xia, Q. Jian, C. Zhao, M. N. Hedhili and H. N. Alshareef, *Adv. Mater.,* 2016, **28**, 77-85.

S16 L. Han, X. Yu and X. W. Lou, *Adv. Mater.,* 2016, **28**, 4601-4605.

S17 Y. Feng, X. Yu and U. Paik, *Chem. Commun.,* 2016*,* **52**, 6269-6272.

S18 X. Yu, Y. Feng, B. Guan, X. W. Lou and U. Paik, *Energy Environ. Sci.,* 2016, **9**, 1246-1250.

S19 W. Ahn, M. G. Park, D. U. Lee, M. H. Seo, G. Jiang, Z. P. Cano, F. M. Hassan and Z. Chen, *Adv. Funct., Mater.* 2018, **28***,* 1802129.

S20 H. Zou, C. Yuan, H. Zou, T. Cheang, S. Zhao, U. Y. Qazi, S. Zhong, L. Wang and A. Xu, *Catal. Sci. Technol.,* 2017, **7**, 1549-1555.

S21 C. Xuan, J. Wang, W. Xia, Z. Peng, Z. Wu, W. Lei, K. Xia, H. L. Xin and D. Wang, *ACS Appl. Mater. Interfaces,* 2017, **9**, 26134-26142.

S22 X. Xu, H. Liang, F. Ming, Z. Qi, Y. Xie and Z. Wang, *ACS Catal.,* 2017, **7**, 6394-6399.

S23 L. Feng, A. Li, Y. Li, J. Liu, L. Wang, L. Huang, Y. Wang and X. Ge, *ChemPlusChem,* 2017, **82**, 483-488.

S24 X. Zou, A. Goswami and T. Asefa, *J. Am. Chem. Soc.,* 2013, **135**, 17242-17245.
S25 X. Yu, M. Zhang, W. Yuan and G. Shi, *J. Mater. Chem. A,* 2015, **3**, 6921-6928.
S26 F. Song and X. Hu, *J. Am. Chem. Soc.,* 2014, **136**, 16481-16484.
S27 Y. Li and C. Zhao, *ACS Catal.,* 2017, **7**, 2535-2541.
S28 C. Dong, X. Yuan, X. Wang, X. Liu, W. Dong, R. Wang, Y. Duan and F. Huang, *J. Mater. Chem. A,* 2016, **4**, 11292-11298.
S29 M. Gong, Y. Li, H. Wang, Y. Liang, J. Z. Wu, J. Zhou, J. Wang, T. Regier, F. Wei and H. Dai, *J. Am. Chem. Soc.,* 2013, **135**, 8452-8455.
S30 R. Liu, Y. Wang, D. Liu, Y. Zou and S. Wang, *Adv. Mater.,* 2017, **29**, 1701546.
S31 N. Han, F. Zhao and Y. Li, *J. Mater. Chem. A,* 2015, **3**, 16348-16353.
S32 C. Guan, X. Liu, A. M. Elshahawy, H. Zhang, H. Wu, S. J. Pennycook and J. Wang, *Nanoscale Horizon.,* 2017, **2**, 342-348.
S33 C. Sun, Q. Dong, J. Yang, Z. Dai, J. Lin, P. Chen, W. Huang and X. Dong, *Nano. Res.,* 2016, **8**, 2234-2243.
S34 M. Łukaszewski, M. Soszko, A. Czerwiński, *Int. J. Electrochem. Sci*., 2016, **11**, 4442-4469.
S35 T. Liu, P. Li, N. Yao, T. Kong, G. Cheng, S. Chen and W. Luo, *Adv. Mater.,* 2019. 1806672.
S36 G. Rajeshkhanna, T. I. Singh, N. H. Kim and J. H. Lee, *ACS Appl. Mater. Interfaces*, 2018, **10**, 42453-42468.
S37 K. N. Dinh, P. Zheng, Z. Dai, Y. Zhang, R. Dangol, Y. Zheng, B. Li, Y. Zong and Q. Yan, *Small,* 2018, **14**, 1703257.
S38 L. Yan, Y. Ren, X. Zhang, Y. Sun, J. Ning, Y. Zhong, B. Teng and Y. Hu, *Nanoscale,* 2019, **11**, 20797-20808.
S39 S. Dutta, A. Indra, Y. Feng, T. Song and U. Paik, *ACS Appl. Mater. Interfaces,* 2017, **9**, 33766-33774.
S40 a) M. A. Sayeed and A. P. O'Mullane, *ChemPhysChem*, 2019, **20**, 3112-3119; b) D. A. Salvatore, K. E. Dettelbach, J. R. Hudkins and C. P. Berlinguette, *Sci. Adv.,* 2015, **1**, 1400215.
S41 Y. Feng, X. Yu and U. Paik, *Sci. Rep.,* 2016, **6**, 34004.
S42 L. He, B. Cui, B. Hu, J. Liu, K. Tian, M. Wang, Y. Song, S. Fang, Z. Zhang and Q. Jia, *ACS Appl. Energy Mater.,* 2018, **1**, 3915-3928.
S43 L. M. Cao, Y. W. Hu, S. F. Tang, A. Iljin, J. W. Wang, Z. M. Zhang and T. B. Lu, *Adv. Sci.,* 2018, **5**, 1800949.
S44 Q. Liang, L. Zhong, C. Du, Y. Zheng, Y. Luo, J. Xu, S. Li and Q. Yan, *Adv. Funct. Mater.,* 2018, **28**, 1805075.
S45 Y. Yang, Z. Lin, S. Gao, J. Su, Z. Lun, G. Xia, J. Chen, R. Zhang and Q. Chen, *ACS Catal.,* 2016, **7**, 469-479.
S46 C. Guan, X. Liu, A. M. Elshahawy, H. Zhang, H. Wu, S. J. Pennycook and J. Wang, *Nanoscale Horizon.,* 2017, **2**, 342-348.
S47 A. Kumar and S. Bhattacharyya, *ACS Appl. Mater. Interfaces,* 2017, **9**, 41906-41915.
S48 B. Singh and A. Indra, *ACS Appl. Nano Mater*., 2020, **3**, 6693-6701.
S49 A. Indra, U. Paik and T. Song, *Angew. Chem. Int. Ed*., 2018, **57**, 1241-1245.
S50 a) J. Duan, S. Chen and C. Zhao, *Nat. Commun.*, 2017, **8**, 15341; b) F. D. Speck, K. E. Dettelbach, R. S. Sherbo, D. A. Salvatore, A. Huang and C. P. Berlinguette, *Chem.*, 2017, **2**, 590-597.

S51 a) C. Ray, S. C. Lee, B. Jin, A. Kundu, J. H. Park and S. C. Jun, *ACS Sustain. Chem. Eng.*, 2018, **6**, 6146-6156; b) P. Wang, Z. Pu, Y. Li, L. Wu, Z. Tu, M. Jiang, Z. Kou, I. S. Amiinu and S. Mu, *ACS Appl. Mater. Interfaces*, 2017, **9**, 26001-26007.

S52 A. Indra, P. W. Menezes, C. Das, D. Schmeißer and M. Driess, *Chem. Commun*., 2017, **53**, 8641-8644.

S53 P. W. Menezes, A. Indra, V. Gutkin and M. Driess*, Chem. Commun*., 2017*,* **53***,* 8018-8021.

S54 A. Indra, P. W. Menezes, C. Das, C. Göbel, M. Tallarida, D. Schmeißer and M. Driess, *J. Mater. Chem. A,* 2017, **5**, 5171-5177.

S55 A. Indra, P. W. Menezes, N. R. Sahraie, A. Bergmann, C. Das, M. Tallarida, D. Schmeißer, P. Strasser and M. Driess, *J. Am. Chem. Soc.,* 2014, **136**, 17530-17536.